Science in China Series D: Earth Sciences

www.scichina.com
earth.scichina.com
www.springerlink.com

Magnetic properties related to thermal treatment of pyrite

WANG Lei[1,2], PAN YongXin[1,3†], LI JinHua[1,2] & QIN HuaFeng[1,2]

[1] Paleomagnetism and Geochronology Laboratory (SKL-LE), Institute of Geology and Geophysics, Chinese Academy of Sciences, Beijing 100029, China;
[2] Graduate University, Chinese Academy of Sciences, Beijing 100049, China;
[3] Key Laboratory of the Study of Earth's Deep Interior, Institute of Geology and Geophysics, Chinese Academy of Sciences, Beijing 100029, China

Detailed rock magnetic experiments were conducted on high-purity natural crystalline pyrite and its products of thermal treatments in both argon and air atmospheres. In argon atmosphere (reducing environment), the pyrite is altered by heating to magnetite and pyrrhotite; the latter is stable in argon atmosphere, and has coercive force and coercivity of remanence of ~20 and ~30 mT, respectively. Whereas in air, the pyrite is ultimately oxidized to hematite. First order reversal curve (FORC) diagram of the end product shows that the remanence coercivity of hematite is up to ~1400 mT. The corresponding thermal transformation process of pyrite in air can be simply summarized as pyrite→pyrrhotite→magnetite→hematite. These results are helpful for understanding of sedimentary magnetism, secondary chemical remanence and meteorolite magnetic properties.

pyrite, pyrrhotite, magnetite, hematite, thermal alteration, rock-magnetic properties

1 Introduction

Pyrite is the most stable iron sulphide in reducing environment[1]. It plays an important role in the sulfur and iron cycles of marine sediments[2]. Because of its importance and prevalence, a number of researches were carried out on pyrite by many workers from the aspects of mineralogy, mineral phase transformation and thermal decomposition[3−10]. Hong and Fegley[5] conducted the experiment on pyrite decomposition in 100 μL/L O_2—CO_2 gas mixture and noted that at lower temperatures (392—460℃), hematite and pyrrhotite were the oxidation and decomposition products of pyrite, while at higher temperatures (484—538℃), no detectable hematite was observed in the products. Others also found that pyrrhotite and hematite are the main decomposition and oxidation products of pyrite[3,4,6]. Conversion of monoclinic pyrrhotite to hexagonal pyrrhotite was also observed[4]. On the other hand, formation of iron sulphate as intermediate product was noted[7,8]. Hu et al.[9] proposed the decomposition and oxidation processes of pyrite as follows: pyrite→pyrrhotite→troilite→iron for the transformation of pyrite in inert atmospheres. He and his coworkers also concluded that as oxidation products, hematite forms at high temperatures (900—1000℃) with high oxygen concentration, while magnetite forms at higher temperature with low oxygen concentration. Gillett[10] studied the relation of pyrrhotite, magnetite and pyrite and reported that under reducing conditions, pyrrhotite can form at the expense of magnetite in the presence of sufficient pyrite even under very mild conditions.

However, the magnetic properties of pyrite and its decomposition and oxidation products are rather rarely studied, mainly because pyrite is paramagnetic at room

Received January 22, 2008; accepted May 14, 2008
doi: 10.1007/s11430-008-0083-7
†Corresponding author (email: yxpan@mail.iggcas.ac.cn)
Supported by the National Science Foundation of China (Grant Nos. 40221402, 40325011, 40634024) and the Chinese Academy of Sciences Project (Grant No. KZCX3-SW-150)

temperature, which does not carry remanence and is often overlooked by researchers[11,12]. Actually, its thermal treatment products are strong ferrimagnetic (e.g., pyrrhotite, magnetite) or canted antiferromagnetic (e.g., hematite) minerals, which have great capacity of carrying remanence. These transformations make environment magnetic signals more complicated[1] and strongly influence the reliability of paleomagnetic signals[12]. Therefore, rock magnetic properties of pyrite and associated thermal alteration are of great importance for correct interpretation of sedimentary magnetism and paleomagnetic results. Moreover, iron-sulfide was also found in Martian meteorolite (ALH84001)[13]. Thus, systematic studies of rock magnetism of pyrite and other iron-sulfide are also needed for understanding other celestial bodies' magnetism and environmental evolution in solar system[13,14].

We carried out investigations on natural pyrite sample and its related thermal treatment products using rock magnetism methods in conjunction with other non-magnetic approaches. Thermomagnetic analyses (χ-T and J-T curve) provide a real time and sensitive method for detecting the magnetic mineral alterations during thermal treatment. A combination of room-temperature and low-temperature rock-magnetic experiments (e.g., first order reversal curves, FORC, hysteresis loops and low-temperature transition of remanence) provides information of mineralogy, grain size and magnetic interaction of magnetic minerals[11,15−17]. Besides, in this study, we conducted X-ray diffraction (XRD) analysis on pyrite and its heated products to unravel its thermal transformation processes.

2 Material and method

The studied natural pyrite sample was from the Yunfu City, Guangdong Province, China. XRD analysis confirmed its high purity and crystalline. The sample was ground to 0.074 mm powder in agate muller and the powder samples (named Py1, Py2, Py3, Py4) were used for rock-magnetic studies and the XRD analysis.

Thermal treatment of Py1 and Py2 in argon atmosphere (reducing environment) was conducted on a KLY-3s Kappa-bridge with temperature device CS-3. Samples were heated at a rate of 11℃·min^{-1} and the temperature-dependence of magnetic susceptibility (χ-T) curves was measured. Sample Py1 was stepwise heated to maximum temperatures of 420, 550, 610 and 700℃ (Figure 1). Sample Py2 was heated 4 times up to 700℃.

Thermal treatment of Py3 and Py4 in air (oxidation environment) was conducted on a Magnetic Measurement Variable Field Transitional Balance (VFTB) using a constant field of 1 T. The J-T curves were measured at a heating rate of 40℃min^{-1}. Similar to the χ-T curve measurements, sample Py3 was stepwise heated and sample Py4 was heated 6 times up to 700℃.

Hysteresis loops and related parameters (saturation magnetization M_s, saturation remanence M_{rs}, coercive force B_c, coercivity of remanence B_{cr}) were measured on a MicroMag AGM Model 2900 and a VFTB. FORC diagrams were conducted on the MicroMag 2900. The low-temperature experiments were performed on MPMS XL (Quantum Design) The sample was imparted a saturation isothermal remanence (SIRM) in a field of 5 T at 300 K, then the remanence of both the cooling (300−5 K) and warming (5−300 K) cycles was measured at a temperature interval of 5 K between 40 and 300 K and that of 2 K between 30 and 40 K. The contents of carbon and sulfur solid released during heating were analyzed using CS-902T Carbon & Sulfur Analyzer. The XRD analyses were performed on D-MAX2400 X-Ray diffractometer. The diffraction was scanned between 5° and 70° with 2θ at a scan speed of 4° min^{-1}, using a voltage of 40 kV and current of 40 mA.

3 Results

3.1 Temperature-dependence of low-field magnetic susceptibility

Figure 1 shows the χ-T curves of stepwise heating of sample Py1 in argon. The Curie temperature and phase transformation of the sample can be easily detected by the χ-T curve[18]. From room temperature to 355℃ (Figure 1(a)), the susceptibility decreases, obeying the Curie-Weiss law. From 355 to 420℃, the susceptibility increases slightly (Figure 1(a)), which suggests that some new magnetic minerals may have been produced. Starting from 440℃, there is a sharp increase of susceptibility, reaching the maximum at 550℃ (Figure 1(b)), which is approximately 400 times the initial value. It indicates that strong magnetic mineral phase is newly formed in sample. At the same time, irritating gas (possibly SO_2) is smelled. The susceptibility decreases sharply between 560 and 590℃ (Figure 1(c)), indicating the generation of magnetite. The small amount of

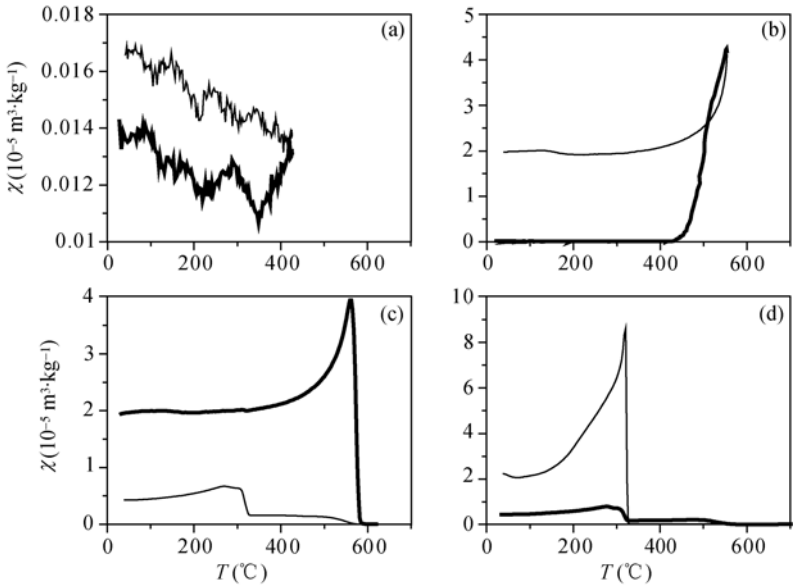

Figure 1 χ-T curves of stepwise heating pyrite (sample Py1) in argon atmosphere. (a)—(d) represent the runs of 420, 550, 610, and 700℃, respectively. Coarse and thin lines refer to heating and cooling curves, respectively.

oxygen is possibly derived from the pyrite crystals and residual of sample holder[19]. However, the corresponding cooling curve indicates that the newly formed magnetite is quickly reduced to become pyrrhotite (Figure 1(c)) as indicated by a sharp increase of susceptibility around 320℃[19,20]. Some yellow solid was released at this stage, the CS-902T Carbon & Sulfur Analyzer confirmed that it is pure sulfur. It is possible that the desulphurization reaction leads to the breakdown of pyrite and the production of pyrrhotite between 550 and 610℃, and the reaction can be simply described as

$$7FeS_2 \rightarrow Fe_7S_8 + 6/nS_n \quad (1)$$

where S_n represents for allotropic species of sulfur, and n could be 2 to 8[9].

The susceptibility increased sharply at 320℃ on the cooling curve of the 700℃ run (Figure 1(d)), indicative of the character of pyrrhotite[7,19]. During cooling, the susceptibility value of the 320℃ peak of this step (Figure 1(d)) is 12 times higher than that of the 610℃ run (Figure 1(c)), suggesting that much more pyrrhotite was produced during the 700℃ run.

Sample Py2 was repeatedly heated to 700℃ for 4 times and the χ-T curves are shown in Figure 2. During the first 700℃ run (Figure 2(a)), the heating curve suggests the new formation of magnetite, while the cooling curve exhibits a rapid increase in susceptibility at 320℃, indicative of pyrrhotite formation. During the second 700℃ run (Figure 2(b)), both the heating and cooling curves signal the Curie point of pyrrhotite at 320℃, while the susceptibility between 200 and 280℃ in the heating curve may indicate the λ-transition[21,22], which is part of monoclinic pyrrhotite change to hexagonal pyrrhotite. The subsequent two 700℃ runs (Figures 2(c) and (d)) show almost all reversible heating and cooling curves, and the behavior of pyrrhotite.

3.2 High-temperature magnetization and hysteresis loops

Figure 3 shows the J-T curves of the pyrite sample Py3, which was stepwise heated in the oxidation environment (in air). The corresponding hysteresis loops are shown in Figure 4. The magnetization increased sharply above 400℃ (Figure 3(a)) and reached its maximum at 518℃ (Figure 3(b)), indicating that strong magnetic minerals have been produced. The room-temperature hysteresis loop of the thermal product of the 420℃ closed at about 100 mT (Figure 4(a)), which is the character of low-coercivity components. The relatively low values of the coercivity and remanence rations (B_{cr}/B_c = 2.86, M_{rs}/M_s = 0.158) indicate a large PSD grain size of the newly produced minerals[23]. After heating to 550 °C, the magnetic grain size became significantly finer, indicated by the decreased coercivity ratio and increased remanence ratio (B_{cr}/B_c = 1.63, M_{rs}/M_s=0.404 (Figure 4(b))[23]. During the 610 and 700℃ runs (Figures 3(c)

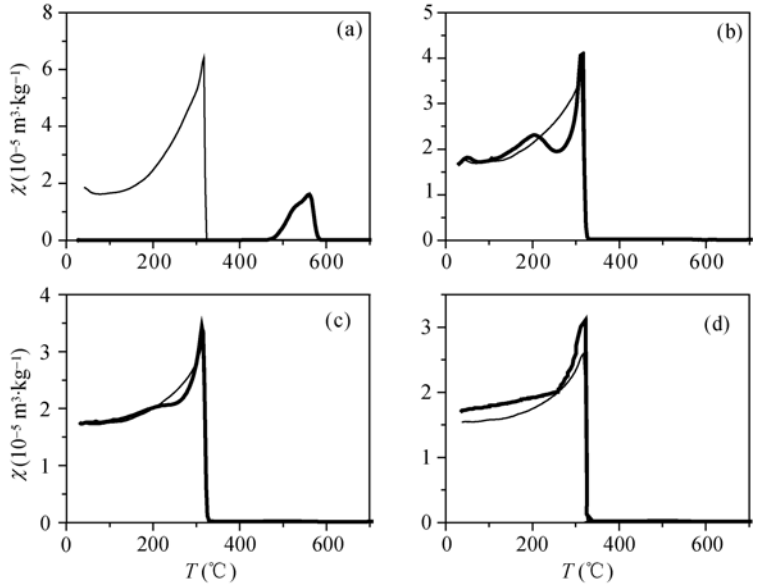

Figure 2 χ-T curves of repeatedly heating pyrite (sample Py2) in argon atmosphere. The sample was heated up to 700℃ for 4 times. (a)—(d) stand for the first to the fourth 700℃ runs. Coarse and thin lines refer to heating and cooling processes, respectively.

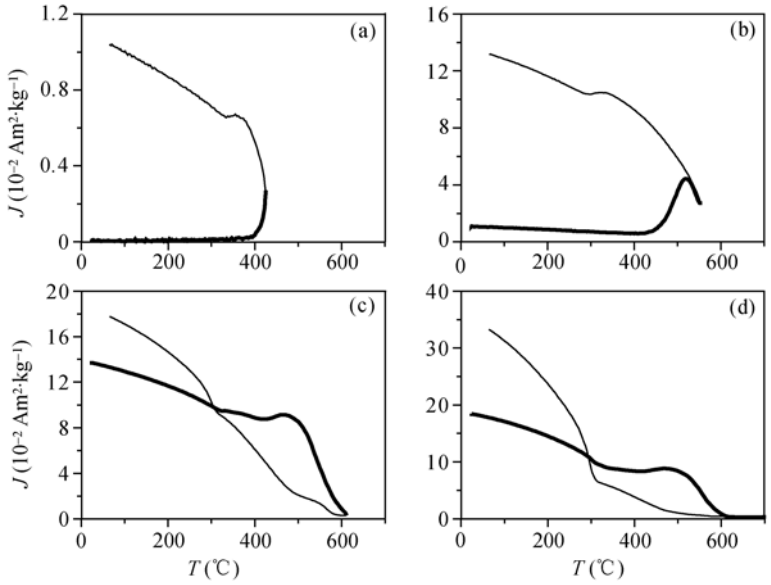

Figure 3 High-temperature magnetization curves of stepwise heating pyrite sample Py3 in air. (a)—(d) represent the runs of 420, 550, 610 and 700℃, respectively. The applied field is 1 T. Coarse and thin lines refer to heating and cooling runs, respectively.

and (d)), the magnetization increased slowly between 420 and 470℃ and decreased sharply between 500 and 600℃, suggesting the production of magnetite. The coercivity of the products of the 610 and 700℃ runs increased significantly, indicated by their room-temperature hysteresis loops closed at 400—600 mT (Figures 4(c) and (d)). The increased coercivity may be due to the newly produced pyrrhotite and magnetite of SD magnetic grain size[24]. The hysteresis parameters indicate that the magnetic grain sizes of the thermal products decreased from PSD to SD with increasing of the heating temperature. All the cooling curves show an inflexion at ~320℃ and the magnetization increased much faster after this temperature than before. This behavior becomes more obvious on the 700℃-run cooling curve (Figure 3(d)). XRD results of the heated sample showed the coexistence of pyrrhotite and pyrite in the 700℃ product.

The pyrite sample Py4 was heated in air to 700℃ for 6 times and the J-T curves are shown in Figure 5. The

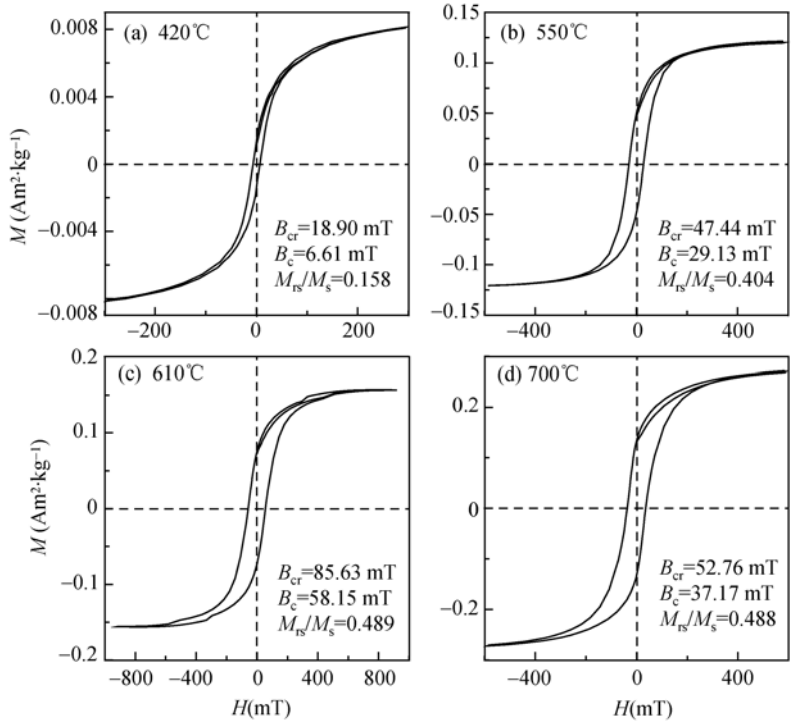

Figure 4 Hysteresis loops of the thermal products of the pyrite sample Py3, which correspond to the *J-T* curves of Figure 3.

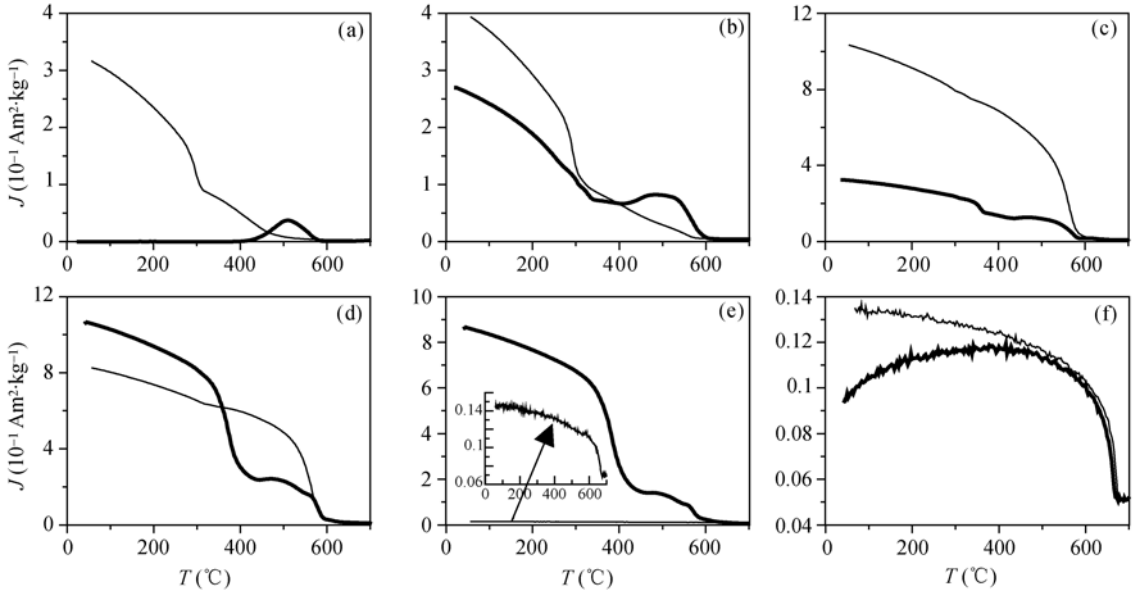

Figure 5 High-temperature magnetizations (*J-T* curves) of repeatedly heated pyrite (sample Py4) in air. The sample was heated up to 700℃ in air for 6 times. (a)—(f) represent the first to the sixth runs. Bold and thin lines refer to heating and cooling processes, respectively.

heating curve of the first 700℃ run is similar to that in argon (Figures 5(a) and 2(a)), indicating the formation of magnetite. The magnetization increased from 550 to 320℃ on the cooling curve, becoming much faster below 320℃ (Figure 5(a)), suggesting the formation of pyrrhotite. The second 700℃ run (Figure 5(b)) shows the behavior of pyrrhotite and magnetite at about 320 and 580℃ on both the heating and cooling curves. During the subsequent 700℃ runs (Figures 5(c)—(e)), the heating curves show the existence of pyrrhotite and magnetite. However, the cooling curves of the third and fourth 700℃ runs (Figures 5(c) and (d)) reveal the dominant presence of magnetite, indicating that pyrrhotite has been transformed to magnetite. The cooling

curve of the fifth run (inset in Figure 5(e)) shows a marked drop in magnetization at about 680℃, the Néel temperature of hematite. This behavior suggests that the original pyrite, and the secondary minerals produced during thermal treatment, such as pyrrhotite and magnetite, all have been oxidated to hematite. The sixth 700℃ run only shows the behavior of hematite (Figure 5(f)), indicating that all the pyrite has been changed to hematite. Both the low-temperature magnetic measurement and XRD analyses confirm that hematite is the only mineral.

The corresponding hysteresis loops of the thermal products examined in Figure 5 are shown in Figure 6. From the first to the fourth 700℃ runs, the room temperature coercivities of the thermal products decrease from 67.7 to 39.2 mT, and the fields, at which the hysteresis loops are closed, decrease from 500 mT to about 200 mT (Figures 6(a) to (d)). The behavior indicates that the thermal products from the first to the fourth 700℃ runs become magnetically softer and softer, con- sistent with the corresponding *J-T* curves (Figures 5(a) and (d)). Magnetite serves as the dominant magnetic mineral in the thermal product of the fourth 700℃ run (Figure 5(d)). The hysteresis loop of the thermal product of the fifth 700℃ run shows pronounced wasp-waisted behavior (Figure 6(e)), which arises from the coexistence of two magnetic mineral components with strongly contrasting coercivities[25,26]. The hysteresis loop of the thermal product of the sixth 700℃ run (Figure 6(f)) clearly shows a potbellied character[27], and the B_c reaches 842.8 mT, indicative of the presence of a high-coercivity phase. Evidence of this phase as hematite comes from the *J-T* curve (Figure 5(f)), the low-temperature magnetic measurement (Figure 7(b)) and XRD analysis.

3.3 Low-temperature magnetic measurements

Low-temperature magnetic experiments were conducted on the end thermal products both in argon and air (Figure 7). The product of the fourth 700℃ run treated in argon (Figure 7(a)) shows a pronounced transition at 34 K, which is the typical characteristic of pyrrhotite[21], and is consistent with its χ-*T* curve (Figure 2(d)). The product of the sixth 700℃ run treated in air shows a marked transition at about 250 K (Figure 7(b)), which is the Morin transition[28] for hematite, and is consistent with its *J-T* curve (Figure 5(f)).

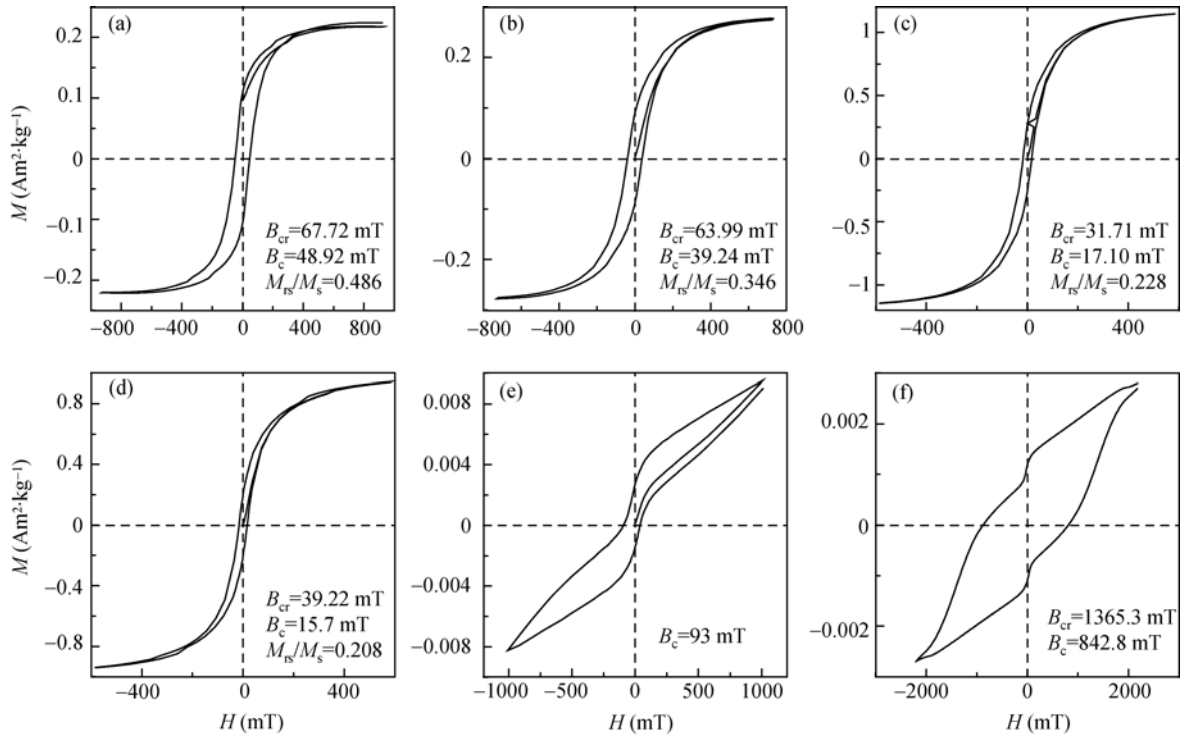

Figure 6 Hysteresis loops of the thermal products of the pyrite sample Py4, which was heated to 700℃ for six times in air by VFTB (Figure 5). Paramagnetic contributions were subtracted for the hysteresis loops shown in ((a)—(d)). The loops shown in ((a)—(e)) were measured by VFTB, and in (f) by MicroMag 2900 AGM.

3.4 FORC diagram

The FORC diagrams can be used to classify magnetic domain, coercivity and interaction between particles[24].The thermal products in argon of sample Py1 stepwise heated to 700℃ (Figure 1(d)) and of sample Py2 of the fourth 700℃ run (Figure 2(d)) in argon show FORC diagrams with closed isolines and lower average coercivity (<60 mT) (Figures 8(a) and (b)), suggesting that the newly produced pyrrhotite is mainly of single domain (SD) size[29]. The FORC diagram of the thermal product of the pyrite sample Py3 stepwise heated to 700℃ in air (Figure 8(c)) shows that the coercivity is higher than the coercivities of the thermal products obtained in argon (Figures 8(a) and (b)), Combined with the hysteresis loops (Figure 3(d)) and XRD analysis (Figure 9(d)), we speculate that this increase in coercivity is due to the mixture of SD pyrrhotite and magnetite. However, the FORC diagram (Figure 8(d)) of the thermal product of the sixth 700℃ run in air (Figure 5(f)) shows that the coercivity increased sharply, and the FORC distributes in the high- and low-coercivity districts. B_c of the high-coercivity district reaches 1400 mT, suggesting that the final thermal product of pyrite in air is SD hematite, which is further confirmed by the XRD analysis (Figure 9(e)). The low-coercivity district may be due to the presence of very little amount of pyrrhotite and magnetite.

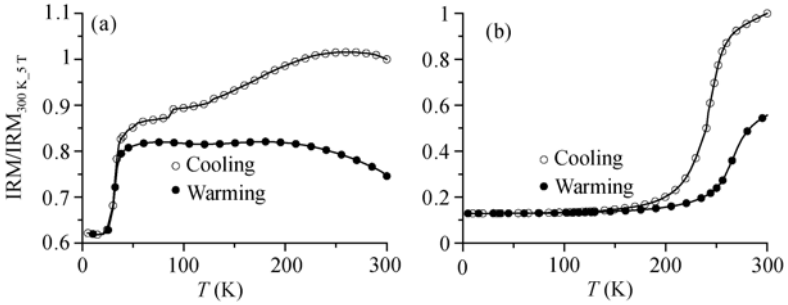

Figure 7 Low-temperature demagnetization (LTD) spectra of the SIRMs of the thermal products of pyrite. (a) represents LTD spectrum of the product of the fourth 700℃ run in argon of sample Py2 (Figure 2(d)); (b) represents that of the product of the sixth 700℃ run in air of sample Py4 (Figure 5(f)).

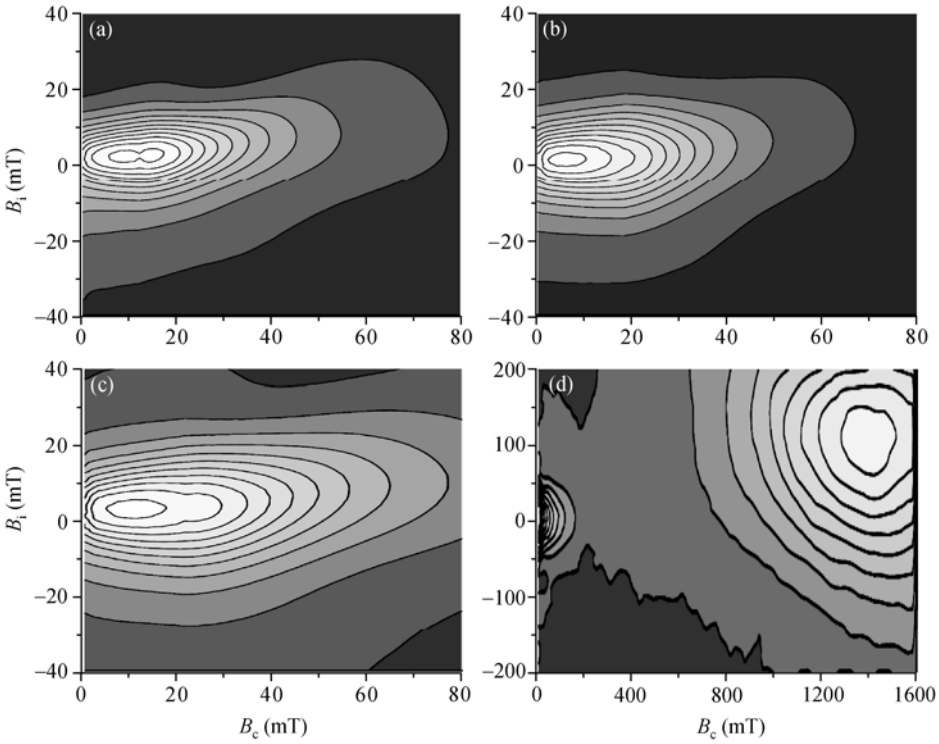

Figure 8 FORC diagrams. B_c represents coercivity force, and B_i the interaction field. (a) FORC of the thermal product of the pyrite sample Py1 stepwise heated to 700℃ in argon; (b) FORC of the thermal product of the pyrite sample Py2 of the fourth 700℃ run in argon; (c) FORC of the product of the pyrite sample Py3 stepwise heated to 700℃ in air; (d) FORC of the product of the pyrite sample Py4 of the sixth 700℃ run in air.

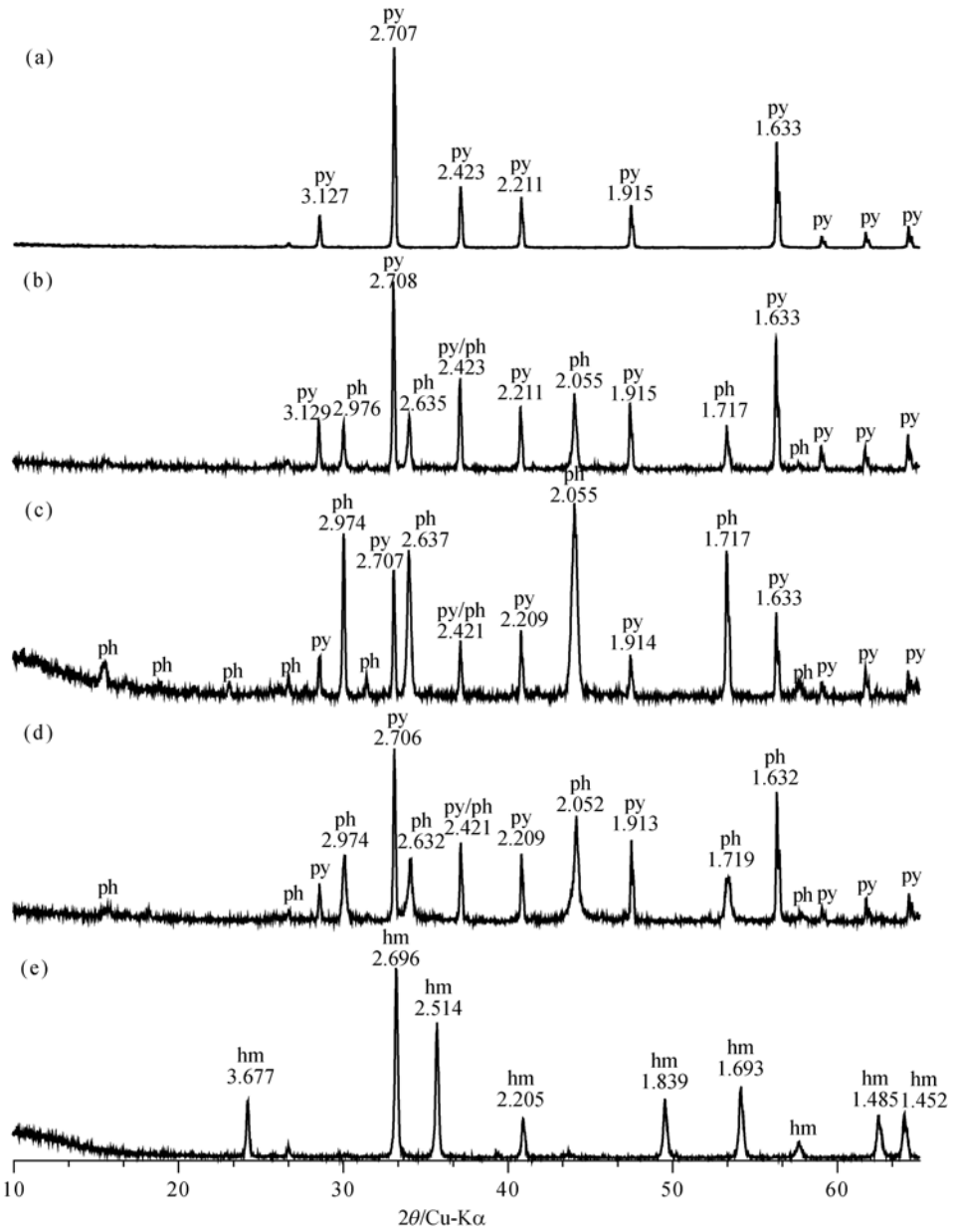

Figure 9 XRD spectra of pyrite and its thermally treated products. (a) Natural pyrite sample; (b) thermal product of the pyrite sample Py1 stepwise heated to 700℃ in argon; (c) product of the pyrite sample Py2 of the fourth 700℃ run in argon; (d) product of the pyrite sample Py3 stepwise heated to 700℃ in air; (e) product of the pyrite sample Py4 of the sixth 700℃ run in air. py, ph, and hm represent pyrite, pyrrhotite, and hematite, respectively.

4 Discussion and conclusions

4.1 Magnetic properties and phase transformation during thermal treatment

The magnetic behavior of pyrite during thermal treatment appears to be very complex. Factors such as temperature, oxygen concentration, particle size, flow condition and the surrounding atmosphere all affect its decomposition and oxidation process[9]. Thermomagnetic analyses serve as powerful methods, which can detail the real time change of pyrite during thermal treatment. Based on the observations of temperature-dependent magnetic susceptibility, Li and Zhang[19] considered pyrrhotite is the thermal product of pyrite.

In our study, in the step by step heating pyrite in argon, the thermal products in argon of the 550 and 610℃ runs (Figures 1(b) and (c)) show significant production of magnetite, and no pyrrhotite is showed by the 550℃

curve (Figure 1(b)). The cooling curve of the 610℃ run (Figure 1(c)) shows that only a little amount of magnetite was stable, and susceptibility increases by 120% at 320℃, which is the T_c of pyrrhotite. We can speculate that magnetite transformed to pyrrhotite. Also pyrrhotite may come from the desulfuration reaction. Li and Zhang[19] considered that magnetite reacted with sulfur and proposed the following reaction

$$Fe_3O_4+5S = 3FeS+2SO_2 \quad (2)$$

However, we suggest that at this stage, there was still unreacted pyrite, as indicated by the XRD results shown in Figure 9(b). Both pyrite and sulfur are strong reducer, we thus suggest that the reaction could be modified to

$$2Fe_3O_4+FeS_2+10/nS_n = Fe_7S_8+4SO_2 \quad (3)$$

There is little magnetite present when stepwise heated to 700℃ (Figure 1(d)). The mass of pyrrhotite indicated from the cooling curve (Figure 1(d)) comes from the decomposition of pyrite. Therefore, in the circumstance of a little residual oxygen present, pyrite will firstly react with oxygen and then produce magnetite. Pyrrhotite will be produced at the expense of pyrite and magnetite when the oxygen is depleted[22]. When the magnetite is run out of, desulfuration reaction leads to the transformation of pyrite to pyrrhotite. The shapes of the thermomagnetic curves (Figures 2(c) and (d)) of monoclinic pyrrhotite are the same as Li and Zhang's[19] and Ferrow and SjÖberg's[7] curves, but are quite different from those reported by Rochette et al.[21, 22] This may be due to different sources of pyrite. The third and fourth 700°C runs in argon show almost all reversible χ-T curves (Figures 2(c) and (d)), suggesting that in the reduced (argon) environment, pyrrhotite is stable[6], and it is of typical SD grain size indicated from the FORC diagram (Figure 8(b)). No greigite (Fe_3S_4) was detected in the thermal products obtained in reduced environment, while only pyrrhotite was detected by the presence of the 30—35 K transition.

The thermal products of pyrite stepwise heated in air show the mixture of magnetite and pyrrhotite (Figures 3(c) and (d)), but only pyrrhotite was detected by the XRD analysis (Figure 9(c)), possibly because the amount of magnetite is too small to be detected by XRD, but its saturation magnetization is large enough and therefore its presence can be clearly reflected by thermomagnetic analyses. Therefore, XRD analysis is suitable for identification of dominant minerals, but possibly less suitable for identifying minor minerals, while mineral magnetic method can effectively identify the signals of minor magnetic minerals. The use of multiple methods could be suggested for unambiguous identification of magnetic minerals.

For the thermal products of the 700℃ runs in air (Figure 5), both the XRD analyses and low-temperature magnetic experiments show that hematite is the final thermal product of pyrite[3—6]. Pyrrhotite as an intermediate phase has been produced (Figures 5(a)—(e)), which is unstable in the oxidation environment. The cooling curves of the third and fourth 700℃ runs show that pyrrhotite was gradually transformed to magnetite. Both the fifth and sixth 700℃ runs (Figures 5(e) and (f)) show that magnetite was oxidated to hematite. Therefore, in the oxidation environment, pyrite was firstly decomposed to pyrrhotite, then pyrrhotite was oxidated to magnetite, and the repeated heating processes lead to the transformation of pyrrhotite and magnetite to hematite. The corresponding transformation sequence can be described as: pyrite → pyrrhotite → magnetite → hematite. The FORC diagram (Figure 8(d)) shows significant high coercivity (1400 mT), which is the character of hematite.

4.2 Geological significance

Pyrite is widely distributed in natural environments. Hydrothermal and other thermal mechanisms often make it oxidated to pyrrhotite, magnetite and/or hematite, all of which have strong capability of carrying remanence, therefore strongly influencing interpretation of paleomagnetic results. If the pyrite-bearing rocks were later heated by the upwelling and/or intrusion of magma, the magnetic field of the magma activity time would be recorded by its thermal products. If the magma activity can be dated, we can partially use the field information. A worse situation is that if the pyrite-bearing rocks were heated by hydrothermal processes for a very long time, no-good chemical and thermal viscous remanences would be acquired, which can mislead the interpretation of paleomagnetic data. Pan et al.[11] noted that thermal alteration of siderite could cause serious problems to such data. Therefore, how to distinguish such contamination by the product of some paramagnetic minerals, such as pyrite and siderite, is a very important issue[30,31].

In addition, iron-sulfide was found in meteorite sam-

ples[13,14]. Systematic study of rock magnetism of pyrite and other iron-sulfides will be of great interests for understanding other celestial bodies' magnetism and environmental evolution in solar system.

The authors thank Tang Jian for kindly giving the natural pyrite sample, and are grateful to Deng Chenglong who significantly improved an earlier manuscript, and also thank Liu Qingsong, Ao Hong and Zhang Chunxia for valuable discussion, and Li Xin for help in the low-temperature magnetic measurements.

1 Schippers A, Jørgensen B B. Oxidation of pyrite and iron sulfide by manganese dioxide in marine sediments. Geochim Cosmochim Acta, 2001, 65(6): 915－922
2 Hu S Y, Deng C L, Appel E, et al. Environmental magnetic studies of lacustrine sediments. Chin Sci Bull, 2002, 47(7): 613－616
3 Jover O, Rochette P, Lorand J P, et al. Magnetic mineralogy of some granites from the French Massif Central: Origin of their low-field susceptibility. Phys Earth Planet Int, 1989, 55: 79－92
4 Fegley B J, Lodders K, Teriman A H, et al. The rate of pyrite decomposition on the surface of venus. ICARUS, 1995, 115: 159－180
5 Hong H, Fegley B J. The kinetics and mechanism of pyrite thermal decomposition. Ber Bunseng Phys Chem, 1997, 101: 1870－1881
6 Jørgensen F R A, Moyle F J. Phases formed during the thermal analysis of pyrite in air. J Therm Ana, 1982, 25: 473－485
7 Ferrow E A, SjÖberg B A. Oxidation of pyrite grains: A mössbauer spectroscopy and mineral magnetism study. Hyp Int, 2005, 163: 95－108
8 Usher C R, Paul K W, Narayansamy J, et al. Mechanistic aspects of pyrite oxidation in an oxidizing gaseous environment: An in situ HATR-IR isotope study. Environ Sci Technol, 2005, 39: 7576－84
9 Hu G, Dam-Johansen K, Wedel S, et al. Decomposition and oxidation of pyrite. Prog Energy Comb Sci, 2006, 32: 295－314
10 Gillett S L. Paleomagnetism of the Notch Peak contact metamorphic aureole, revisited: Pyrrhotite from magnetite+pyrite under submetamorphic conditions. J Geophys Res-Solid Earth, 2003, 108(B9): EPM 9-1
11 Pan Y X, Zhu R X, Banerjee S K. Rock magnetic properties related to thermal treatment of siderate: Behavior and interpretation. J Geophys Res, 2000, 105(B1): 783－794
12 Shi C D, Zhu R X. Applications of reserach of iron sulphides in paleomagnetism and environmental magnetism. Prog Geophy (in Chinese), 2000, 15(3): 91－97
13 Rochette P, Gattacceca J, Chevrier V, et al. Magnetism, iron minerals, and life on Mars. Astrobiology, 2006, 6(3): 423－436
14 Acton G, Yin Q Z, Verosub K L, et al. Micromagnetic coercivity distributions and interactions in chondrules with implications for paleointensities of the early solar system. J Geophys Res, 2007, 112: B03S90
15 Deng C L, Zhu R X, Jackson M J, et al. Variability of the temperature-dependent susceptibility of the Holocene eolian deposits in the Chinese loess plateau: A pedogenesis indicator. Phys Chem Earth, 2001, 26(11-12): 873－878
16 Deng C L, Zhu R X, Verosub K L, et al. Paleoclimatic significance of the temperature-dependent susceptibility of Holocene loess along a NW-SE transect in the Chinese loess plateau. Geophy Res Lett, 2000, 27(22): 3715－3718
17 Liu Q S, Deng C L, Yu Y, et al. Temperature dependence of magnetic susceptibility in an argon environment: Implications for pedogenesis of Chinese loess/palaeosols. Geophys J Int, 2005, 161: 102－112
18 Ao H, Deng C L. Review in the identification of magnetic minerals. Prog Geophys (in Chinese), 2007, 22: 432－442
19 Li H Y, Zhang S H. Detection of mineralogical changes in pyrite using measurements of temperature-dependence susceptibilities. Chin J Geophy (in Chinese), 2005, 48(6): 1384－1391
20 Lotgering F K. On the ferrimagnetism of some sulphides and oxides. Philips Res Rep, 1956, 11: 190－249
21 Rochette P, Fillion G, Mattéi J L, et al. Magnetic transition at 30－34 Kelvin in pyrrhotite: Insight into a widespread occurrence of this mineral in rocks. Earth Planet Sci Lett, 1990, 98: 319－328
22 Rochette P. Metamorphic control of the magnetic mineralogy of black shales in the Swiss Alps: Toward the use of "magnetic isograds". Earth Planet Sci Lett, 1987, 84: 446－456
23 Dunlop D J. Theory and application of the Day plot (Mrs/Ms versus Hcr/Hc) 1. Theoretical curves and tests using titanomagnetite data. J Geophys Res, 2002, 107(B3): EMP 4
24 Roberts A P, Christopher R P, Kenneth L V. First-order reversal curve diagrams: A new tool for characterizing the magnetic properties of natural samples. J Geophys Res, 2000, 105(B12): 28461－28475
25 Deng C L, Zhu R X, Verosub K L, et al. Mineral magnetic properties of loess/paleosol couplets of the central loess plateau of China over the last 1.2 Myr. J Geophys Res, 2004, 109(B1): B01103
26 Roberts A P, Cui Y, Verosub K L. Wasp-waisted hysteresis loops: Mineral magnetic characteristics and discrimination of components in mixed magnetic systems. J Geophys Res, 1995, 100(B9): 17909－17924
27 Tauxe L, Mullender T A T, Pick T. Potbellies,wasp-waists and superparamagnetism in magnetic hysteresis. J Geophys Res, 1996, 101: 571－583
28 Morin F J. Magnetic susceptibility of αFe_2O_3 and αFe_2O_3 with added titanium. Phys Rev, 1950, 78: 819－820
29 Roberts A P, Liu Q, Rowan C J, et al. Characterization of hematite(α-Fe_2O_3), goethite(α-FeOOH), greigite(Fe_3S_4), and pyrrhotite (Fe_7S_8) using first-order reversal curve diagrams. J Geophys Res, 2006, 111(B12S35)
30 Pan Y X, Zhu R X, Liu J M. Chemical-viscous remanent magnetization in the oxidation of siderite and its implications in paleomagnetism. Sci China Ser D-Earth Sci, 1999, 42(4): 442－448
31 Shi C D, Zhu R X, Suchy V, et al. Identification and origins of iron sulfides in Czech loess. Geophys Res Lett, 2001, 28(20): 3903－3906